Channel Classification for Free Space Optical Communication Network based on Machine Learning Techniques

Yousef E. M. Hamouda, Ahmed A. Aljuaidi, and Hassan A. Younis

***Abstract*—Free Space Optical (FSO) communication is an optical communications technology that uses unguided light propagation in free space. Comparing with other wireless network systems, FSO links have high bandwidth, free licensed frequencies, high security, and low transmitted power. Nevertheless, FSO wireless channel suffers from different atmospheric attenuation factors. In this paper, Free Space Optical Channel Classification (FSO-CC) approach is presented to predict the suitability of FSO link. The FSO-CC uses machine learning classifiers to predict the FSO channel status. The classifiers decision depends on the satisfaction of the FSO communication performance such as the minimum received signal to noise ratio, and the transmitter capabilities such as the maximum transmitted power. The features inputs of the proposed classifiers are the distance between the FSO transmitter and receiver nodes, and the current weather conditions. The label output of the proposed classifiers is the channel suitability class. The simulation environment of the proposed FSO-CC scheme is implemented using a real dataset of weather conditions, and actually FSO location nodes. The simulation results show that the proposed FSO-CC efficiently estimates the suitability of FSO wireless channel to use FSO communication or other kinds of communication systems, according to the current weather conditions and distance between the FSO transmitter and receiver nodes. Furthermore, the decision-making feature in the proposed FSO-CC are dynamically controlled. Compared with logistic regression, decision tree, and random forest classifiers, the support vector machine classifier gives better performance in terms of prediction errors, F1 score, precision score, accuracy, score, and recall score.**

***Keywords*— Free Space Optical, Machine Learning, Channel Estimation, Weather Conditions, Classification.**

I. INTRODUCTION

FIXED microwave links have been used to carry the data, video conferencing, real time streaming and Internet traffic. However, the microwave frequencies may not be enough to cope with the constantly increased demands of frequencies and Internet access speeds. Furthermore, the radio spectrum is very crowded, and countries may not have licensed spectrum available to deploy additional wireless links. Therefore, the role of optical communications which is very useful for broadband Internet access has been recently raised [1]. The FSO market is likely to grow at a rate of more than 35% in each of the next five years, rising from $200 million to $2 billion by 2027. In addition, FSO can provide connectivity to the areas without optical fiber cables technology for rapid Internet access, and it provides greater flexibility in the design of optical network architectures with very high speeds that can reach to rates of tens and hundreds of gigabits per seconds [2]. FSO can provide a rapid deployment of wireless access solution with greater bandwidth capacity, higher security features, and lower power consumption, compared with other traditional point-to-point microwave links [3]. However, the FSO connection is affected by atmospheric influences, which limits the sensitivity and achievable data rates with an acceptable Bit Error Rate (BER). Some of these degradations are turbulence, absorption, and scattering [4]. Free Space Optical (FSO) communication uses the lasers beams to transmit the data from one location to another. It can be from a satellite to a ground station, or from a satellite to another satellite, or between different locations on the ground. It is possible to make FSO connections point-to-point, point-to-multi-point, multi-point-to-point, and multi-point-to-multi-point, depending on the different scenarios to establish optical connections [4], [3]. Fig. 1 shows the FSO communication block diagram between two locations on the ground.

Machine Learning (ML) is the technology of developing computer algorithms that are able to emulate human intelligence. It draws on ideas from different disciplines such as artificial intelligence, probability and statistics, computer science, information theory, psychology, databases, control theory, and philosophy. Historically, the inception of machine learning can be traced to the seventeenth century and the development of machines that can emulate human ability to add and subtract by Pascal and Leibni [5].

Manuscript received [22 September 2024]; revised [26 January 2025]; accepted [20 February 2025]. Date of publication [26 February 2025]. (*Corresponding author: Yousef E. M. Hamouda).*

Yousef E. M. Hamouda is an Associate Professor at the Faculty of Computer and Information Technology, Al Aqsa University, Gaza, Palestine (e-mail: ye.hamouda@alaqsa.edu.ps).

Ahmed A. Aljuaidi is MSc. Student at Al Aqsa University, Gaza, Palestine (e-mail: aa.aljuaidi@std.alaqsa.edu.ps).

Hassan A. Younis is MSc. Student at Al Aqsa University, Gaza, Palestine (ha.younis@std.alaqsa.edu.ps).

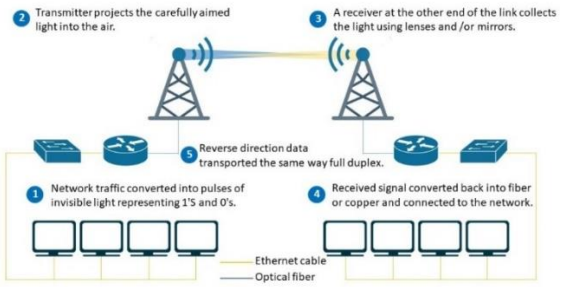

Fig. 1. FSO communication block diagram

Machine learning algorithms build a model based on sample data, known as training data, in order to make predictions or decisions without being explicitly programmed to do so [6]. Modern-day machine learning has two objectives, one is to classify data based on models which have been developed, the other purpose is to make predictions for future outcomes based on these models [7]. ML and Data Mining (DM) often use the same methods and overlap greatly. ML focuses on predicting events through feature in training data. While DM uses ML algorithms to interrogate large databases and discover knowledge hidden in the data [8]. ML has been applied in such diverse fields and applications as email filtering, speech recognition, pattern recognition, computer vision, space craft engineering, finance, entertainment, ecology, computational biology, and biomedical and medical applications [9] [10]. Machine learning will not only be limited to solving problems through similarities in databases, but will extend to artificial intelligence [11]. Recently, ML has become a hot topic in the fiber-based optical communication field as FSO because it eliminates the need for developing complex analytical models for optical communication systems and networks [5]. ML algorithms are widely used to predict the channel impairments for optical communication. However, the research into using ML algorithms in channel estimations is still in its beginning [12]. Hence, Free Space Optical Channel Classification (FSO-CC) scheme is presented in this paper to estimate the suitability of FSO channel to be used for FSO communication, so that the FSO communication performance such as the minimum received Signal to Noise Ratio (SNR), and the transmitter capabilities such as the maximum transmitted power are satisfied. FSO-CC scheme includes an intelligent classification algorithm that uses ML algorithms for channel prediction. The input of the proposed classification algorithm is the distance between the FSO TX and RX nodes, and the weather conditions including fog, snow, and rain [13]. The output of the proposed classification algorithm is the channel suitability class which is either a suitable channel or an unsuitable channel for FSO communication.

This paper consists of seven sections including this section. In Section 2, the related works are explored. The framework of FSO-CC is explained in Section 3. The FSO communication and performance models are introduced in Section 4. In Section 5, the detailed description of the proposed FSC-CC approach is presented. The simulation results are presented and discussed in Section 6. Finally, Section 7 concludes this paper.

II. Related Work

In [1], FSO link is established to communicate between two sites using a beam of light via a Line of Sight (LoS) route to provide an optical connection that allows data rates of 100 Gbit/s across a distance of 1 to 4 km. In [1], the atmospheric impacts of FSO deployment, and the mitigation techniques to avoid it are investigated. The factors that affect the FSO link including geometric loss, atmospheric loss, and ambient noise are considered in [1]. The losses of FSO link depends on the propagation of the laser beam through the atmosphere. It may cause a dropped link between the transmitter and the receiver because of the narrowness of the transmitted beams. As a result, it will be applied to both Radio Frequencies (RF) and FSO communications. However, a real dataset evaluation is not considered in [1]. The study in [14] discusses the effects of air turbulence on optical beams. OptiSystem is used to create the FSO link with air turbulence. Andrews' methods are used to compare the output of the program. The FSO link was active at wavelengths of 850 nm and 1550 nm. The results showed that at 850 nm, turbulence attenuation is greater than at 1550 nm. By using the OptiSystem software, the scintillation is typically specified in the FSO channel [14]. However, the factors of other weather conditions that affect the FSO signal are not considered in [14]. The research in [15] forecasts the visibility and range of the connection as a function of attenuation caused by various cloud situations. The quality of the received signal has been studied as a function of link range, transmitted power, and data rate for various cloud types, in order to ensure proper signal reception while preventing connection failure. The attenuation coefficient has been calculated for different cloud types by taking a range of input signal wavelengths. A minimum value of the Q-factor has been observed in the case of cumulus type clouds among different types of cloud conditions at a data rate of 2.5Gbit/s. If the data rate is increased beyond this rate, proper reception of the signal will not be possible for such a cloud condition [15]. However, other weather conditions are not assumed in [15].

The study in [3] focuses on using the FSO links in satellite communications. Artificial neural network is used to estimate the attenuation coefficient of FSO routes. The Mean Square Error (MSE) is adopted to evaluate the introduced heuristic algorithm in [3]. However, a prediction of new input data is not considered in [3]. In [12], machine learning techniques have been applied to determine different transmission attenuation states in FSO systems. The channel parameters of Amplified Spontaneous Emission (ASE) noise, turbulence, and pointing errors are considered in [12]. The Support Vector Machines (SVM) and Convolutional Neural Network (CNN) machine learning algorithms are used and compared in [12]. The results show that CNN is a good tool for predicting the Optical Signal to Noise Ratio (OSNR) parameter [12]. However, the CNN algorithm mostly consists of several layers, and the training process is more time-consuming and complicated. The research in [16] presents FSO/RF hybrid system that switches the transmission between the FSO and RF according to the present weather conditions. ML

algorithms in [16] is applied to predict the Link Margin (LM) of channel. Meteorological data for rain and fog are considered to estimate and categorize the correlation. However, there are some signs that affect the quality of FSO that are not considered such as temperature and snow. In [17], a study on the FSO communication was conducted in the laboratory. The optical channel in correlation has been replaced by an Optical Turbulence Generating (OTG) chamber to incorporate perturbation effects. The channel coefficients are estimated using Maximum Likelihood Estimation (MLE) and Bayesian estimation methods. MLE is adopted because it is lower complexity [17]. Nevertheless, the technique used in [17] is used to estimate the channel at RX side to reduce the error rate without taking any decision of transmission at TX side. In [18], the effect of dusty weather on FSO propagation is studied. K-Nearest Neighbors (KNN), SVM and CNN algorithms are used to detect light patterns under the influence of a lab simulated desert environment [18].

Unlike all above research, the main contributions of this research are threefold. Firstly, this paper presents Free Space Optical Channel Classification (FSO-CC) scheme to predict the FSO channel suitability for FSO communication with considering the attenuations factors that degrade the received FSO signal. The attention factors include the FSO channel impairments, geometric losses, path losses, and distance separation between the FSO TX and RX nodes. The FSO channel impairments that are considered in FSO-CC scheme are the weather conditions including rain, snow, and fog. Secondly, the FSO-CC scheme adopts two ML algorithms which are the Logistic Regression (LR) and Decision Tree (DT) classifier for prediction and estimation of FSO channel. The evaluations of the two ML algorithms are compared. Thirdly, the proposed FSO-CC scheme are evaluated and analyzed using a real dataset of weather conditions and suggested FSO nodes.

III. FSO-CC Framework

The framework of FSO Channel Classification (FSC-CC) is shown in Fig. 2. The FSO network consists of several locations or places which are called the FSO nodes. Fig. 2 shows six different FSO nodes. The locations and distances among all FSO nodes are assumed to be known at each FSO node. The communication channels among FSO nodes are assumed to have various weather conditions including rain, snow and fog. Each FSO node are able to get the weather conditions in its communication channel.

In good weather conditions, the FSO nodes are connected to each other via FSO links. On the other hand, if the weather conditions are bad, the FSO nodes communicate to each other via any other available communication links such as optical fiber cable or RF transmission. Furthermore, the FSO nodes can search for an acceptable multi-hop FSO path to communicate to each other. Another factor that affects the received FSO signal is the distance between the FSO transmitter node (TX) and the FSO receiver node (RX). If the distance between FSO TX and RX nodes is less than the FSO communication range, the FSO nodes can communicate via FSO links. Otherwise, other communication links are used to perform the communicating between FSO TX and RX nodes. The FSO communication range is the maximum allowed distance between FSO TX and RX nodes after which the FSO performance in terms of Signal to Noise Ratio (SNR) and Bit Error Rate (BER) is degraded under threshold values.

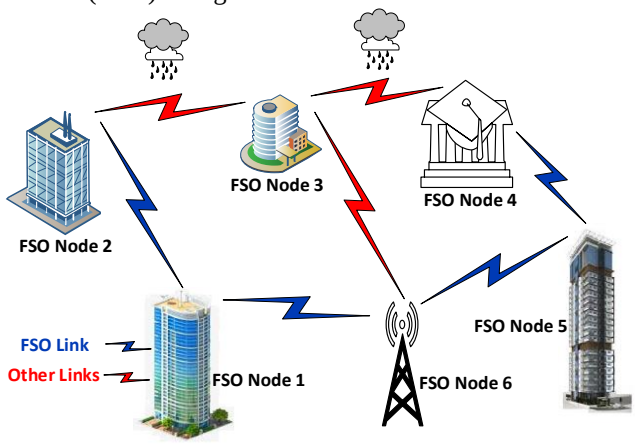

Fig. 2. FSC-CC Framework

IV. FSO Communication Model

In this paper, FSO links are used as the process of communication and data transmission between the TX and RX nodes. As shown in Fig. 3, the design of the FSO links depend on antenna alignment, weather conditions, obstruction, geographic conditions, and many unexpected environmental factors such as fog, rain, clouds, snow, fog, and scintillation. Depending on the various attenuation factors that affect FSO communications, a few of the vital attenuations and losses are explained in the following subsections [19].

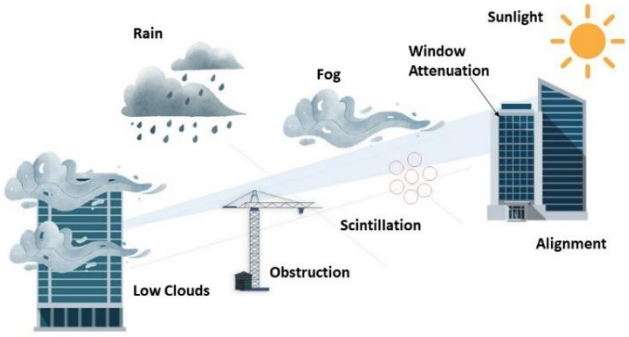

Fig. 3. Factors that affect the FSO communication links

A. Geometric Attenuation

It is the attenuation caused by the reduction of the amount of radiation due to the effect of the distance between the source and destination. Geometric loss is the ratio of the surface area of the receiver aperture to the surface area of the transmitter beam at the receiver [20]. It can be calculated as follows [21]:

$$L_{geo}(s_{TX}, s_{RX}) = 10 \times log\left(\frac{D_T(s_{TX})+d(s_{TX},s_{RX})\times\theta(s_{TX},s_{RX})}{D_R(s_{RX})}\right)^2 (1)$$

where s_{TX} and s_{RX} are the TX and RX FSO nodes, respectively, $D_T(s_{TX})$ is the transmitter aperture diameter in

millimeters (mm), $D_R(s_{RX})$ is the diameter of receiver in mm, $d(s_{TX}, s_{RX})$ is the distance between the TX and RX FSO nodes in kilometers (km), and $\theta(s_{TX}, s_{RX})$ is the beam divergence angle between the transmitter and receiver in mm.rad/km.

B. Atmospheric Attenuation

Atmospheric attenuation is defined as the process by which some or all of the energy of an electromagnetic wave is lost when passing through the atmosphere. Thus, the signal degradation and attenuation of the FSO system link is caused by the atmosphere in several ways, including absorption, scattering and scintillation. All of these effects vary over time and depend on current local conditions and weather [22].

Visibility is an important decider for users planning deployment of FSO. A 5% contrast means that 95% of the visible light is being scattered/absorbed by the atmosphere (i.e. it is attenuated). AND the 5% of visible light coming to you is no more than 13 dB down, or else you would not be able to see the object with your naked eye. So, if you can see an object in the fog, it is no more than 13 dB "away" from you [21]. The Kim model gives the fog losses (in dB) as [23]:

$$L_{fog}(s_{TX}, s_{RX}) = 10 \times log\left(e^{\delta(s_{TX}, s_{RX}) \times d(s_{TX}, s_{RX})}\right) \quad (2)$$

where $d(s_{TX}, s_{RX})$ is between the TX and RX FSO nodes in km, and $\delta(s_{TX}, s_{RX})$ is total extinction coefficient between the TX and RX FSO nodes. The total extinction coefficient is modelled as:

$$\delta(s_{TX}, s_{RX}) = \left(\frac{3.91}{V(s_{TX}, s_{RX})}\right) \times \left(\frac{\lambda}{550}\right)^{-\Psi} \quad (3)$$

where $V(s_{TX}, s_{RX})$ is the visibility in km, λ is the wavelength in nanometres (nm), and Ψ is constant parameters related to the particle size distribution and the visibility and is calculated as:

$$\Psi = \begin{cases} 1.6 & V \geq 50 \\ 1.3 & 6 \leq V < 50 \\ 0.16V + 0.34 & 1 \leq V < 6 \\ V - 0.5 & 0.5 \leq V < 1 \\ 0 & V < 0.5 \end{cases} \quad (4)$$

C. Rain Attenuation

The rain attenuation is the attenuation caused by passing through areas where it rains and affects and weakens the signal quality. The rain rate is an essential parameter for determining rain attenuation [24]. The rain loss in dB is calculated as follows [25]:

$$L_{rain}(s_{TX}, s_{RX}) = K \times R^{\alpha}(s_{TX}, s_{RX}) \times d(s_{TX}, s_{RX}) \quad (5)$$

where R is the rain fall rate in mm/hour (mm/h), $d(s_{TX}, s_{RX})$ is between the TX and RX FSO nodes in km, K is 1.58, and α is 0.63.

D. Snow Attenuation

The droplets of wet and dry snow cause attenuation for the FSO signals. The wet and dry snow losses (in dB) are calculated as follows [25]:

$$L_{snow}(s_{TX}, s_{RX}) = \alpha \times S^{b}(s_{TX}, s_{RX}) \times d(s_{TX}, s_{RX}) \quad (6)$$

where S is the wet or dry snow fall rate in mm/h, $d(s_{TX}, s_{RX})$ is distance between the TX and RX FSO nodes in km, and α and b are specified by:

$$\alpha = \begin{cases} 1.02 \times 10^{-4} \times \lambda + 3.79, & for\ Wet\ Snow \\ 5.42 \times 10^{-5} \times \lambda + 5.50, & for\ Dry\ Snow \end{cases} \quad (7)$$

$$b = \begin{cases} 0.72, & for\ Wet\ Snow \\ 1.38, & for\ Dry\ Snow \end{cases} \quad (8)$$

E. FSO System Noises

Noises is undesirable signals that interrupt the FSO signal. The main source of the noises is the electronic components. Therefore, noises cannot be avoided. Signal to Noise Ratio (SNR) is affected by the noises the receiver side [26]. The shot and thermal noises are the key noise types [27].

1) Shot Noise

The shot noise is the quantum noise that is generated by internal or external sources. The random movement of semiconductor carries (i.e. electronics and holes) in the electronic elements generate the internal source of shot noise. On the other hand, the external source of shot noise is produced by the background radiation at the receiver side. The shot noise is calculated using the following formula [26, 28]:

$$\sigma^2_{shot}(s_{RX}) = 2 \times q \times G_i \times i_M \times F(G_i) \times BW \quad (9)$$

where BW is the bandwidth in Hz, q is the electron charge in C, G_i is the photodetector multiplication gain at the FSO RX node, $F(G_i)$ is the photodetector excess noise factor at the FSO RX node, and i_M is the average value of total multiplied output current which is computed by:

$$i_M = G_i \times s(s_{RX}) \times P_R(s_{RX}) \quad (10)$$

where $P_R(s_{TX}, s_{RX})$ is the received power at FSO RX node in W and $s(s_{RX})$ is photodiode sensitivity in A/W.

2) Thermal Noise

The thermal noise Johnson or Nyquist Noise that is caused by the thermal irritation of internal electrons in the electrical conductor inside the detecting receiver. It is given by [26, 28]:

$$\sigma^2_{thermal}(s_{RX}) = \left(\frac{4 \times k \times Temp \times BW}{R_{load}(s_{RX})}\right) \quad (11)$$

where $R_{load}(s_{RX})$ is the amplifier load resistance, k Boltzmann constant, and $Temp$ is the absolute temperature. The total noise at the FSO RX node is given by:

$$\sigma^2_{total}(s_{RX}) = \sigma^2_{shot}(s_{RX}) + \sigma^2_{thermal}(s_{RX}) \quad (12)$$

F. The FSO Received Power

The received power at the FSO RX node in dBw is given by [29]:

$$P_R(s_{RX}) = 10 \times log\left[P_T(s_{TX}) \times G_T(s_{TX}) \times G_R(s_{RX}) \times L_{FS}(s_{TX}, s_{RX}) \times L_{sys}(s_{TX}, s_{RX})\right] - L_{AT}(s_{TX}, s_{RX}) \quad (13)$$

where $P_T(s_{TX})$ is the FSO transmitted power in W at FSO TX node, $G_T(s_{TX})$ is the antenna gain at FSO TX node, $G_R(s_{RX})$ is the antenna gain at FSO RX node, $L_{FS}(s_{TX}, s_{RX})$ is

the free space propagation loss between the FSO TX and RX nodes, $L_{sys}(s_{TX}, s_{RX})$ is the system losses, and $L_{AT}(s_{TX}, s_{RX})$ is the total FSO atmospheric losses between the FSO TX and RX nodes in dB. $G_T(s_{TX})$, $G_R(s_{RX})$, $L_{FS}(s_{TX}, s_{RX})$, $L_{sys}(s_{TX}, s_{RX})$, and $L_{AT}(s_{TX}, s_{RX})$ are given by [30]:

$$G_T(s_{TX}) = \left(\frac{\pi \times D_T(s_{TX})}{\lambda}\right)^2 \quad (14)$$

$$G_R(s_{RX}) = \left(\frac{\pi \times D_R(s_{RX})}{\lambda}\right)^2 \quad (15)$$

$$L_{FS}(s_{TX}, s_{RX}) = \left(\frac{\lambda}{4 \times \pi \times d(s_{TX}, s_{RX})}\right)^2 \quad (16)$$

$$L_{sys}(s_{TX}, s_{RX}) = \zeta_T(s_{TX}) \times \zeta_R(s_{RX}) \times L_{pT}(s_{TX}) \times L_{pR}(s_{RX}) \quad (17)$$

$$L_{AT}(s_{TX}, s_{RX}) = L_{geo}(s_{TX}, s_{RX}) + L_{rain}(s_{TX}, s_{RX}) + L_{snow}(s_{TX}, s_{RX}) + L_{fog}(s_{TX}, s_{RX}) \quad (18)$$

where $D_T(s_{TX})$ is the TX aperture diameters, $D_R(s_{RX})$ is the aperture diameter of FSO RX node, $\zeta_T(s_{TX})$ and $\zeta_R(s_{RX})$ are the losses because of imperfect optical components at the FSO TX and RX nodes, respectively, and $L_{pT}(s_{TX})$ and $L_{pR}(s_{RX})$ are the pointing losses at the FSO TX and RX nodes, respectively.

G. The FSO Performance

The FSO performance is measured by the Signal to Noise Ratio (SNR) and the Bit Error Rate (BER) at the FSO RX node. In the following subsection, these performance metrics are explained.

1) Signal to Noise Ratio (SNR)

The Signal to Noise Ratio (SNR) at the FSO RX node is the ration between the average signal power to the average noise power and is given by [28]:

$$SNR(s_{RX}) = \frac{[s(s_{RX}) \times P_R(s_{RX})]^2}{\sigma^2_{total}(s_{RX})} \quad (19)$$

2) The Bit Error Rate (BER)

The Bit Error Rate (BER) at the FSO RX node consider using None Return to Zero-On-Off Keying (NRZ-OOK) modulation technique is given by [31], [32]:

$$BER(s_{RX}) = \frac{1}{2} \times erfc\left(\frac{\sqrt{SNR(s_{RX})}}{2\sqrt{2}}\right) \quad (20)$$

where erfc is the complementary error function.

V. Detailed Description of the Proposed FSC-CC Approach

In this section, the types, categories and names of the Machine Learning (ML) algorithms is presented. After that, a detailed description of the introduced FSC-CC scheme is explained.

A. Machine Learning Estimating and Predication Techniques

Machine Learning (ML) algorithms are adopted in this research to predict the suitability of wireless channel to use FSO communications in the presence of real environmental factors and weather conditions. A ML model is a mathematical representation of things and their relationships to each other. It is an expression of an algorithm for a large number of datasets to find patterns or make predictions. The learning algorithm detects patterns within the training data, and outputs an ML model that captures these patterns and predicts the new data. As shown in Fig. 4, ML can be divided into three main categories depending on the nature of the existing data [33].

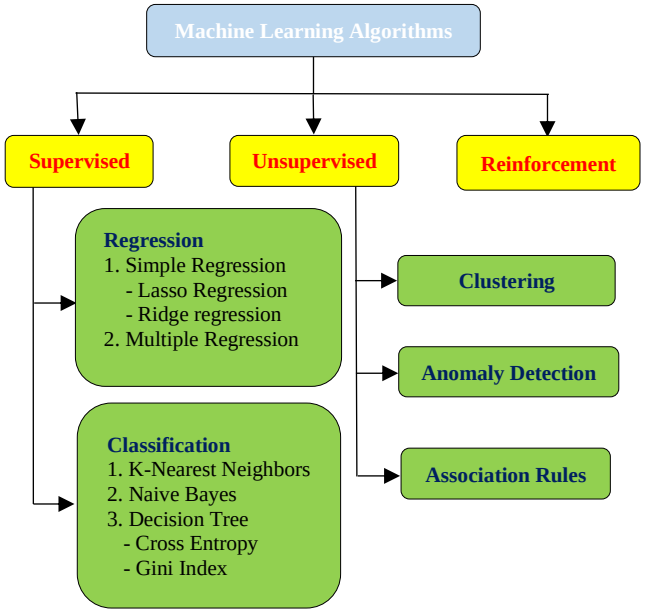

Fig. 4. ML Algorithms Categories.

In supervised learning, the computer is provided with inputs that are labeled with their desired output. The purpose of this method is to enable the algorithm to "learn" by comparing its actual output with the "taught" outputs to find errors and modify the model accordingly. Thus, supervised learning uses patterns to predict label values on additional, and unlabeled data (e.g. classification and regression). On the other hand, the unsupervised learning involves using a model to describe or extract relationships in the data. Comparing with supervised learning, the unsupervised learning operates only on input data without target outcomes or variables. As such, the teacher does not correct the model, as in supervised education. Also, in unsupervised learning there is no teacher or debugger, and the algorithm must learn how to understand the data without such evidence (e.g. clustering and estimation of probability density function). Reinforcement learning is the only possible way to train programs or machines to perform at high levels. Reinforcement learning describes a class of problems in which a worker operates in an environment and must learn how to work using feedback. In this type, the learner is not told what actions to take, but instead has to find out which actions work best of efficiency, through his experience [34]. Semi-supervised learning is supervised learning, in which the training data contains a small number of tagged examples, and a large number of unlabeled examples.

Supervised Learning models are further classified into two categories which are classification and regression. In the classification, a classifier model is designed to classify the dataset into different categories. Each category is assigned with a label. Some popular classification algorithms are Naive Bayes, K-Nearest Neighbors (KNN), and Decision Tree (DT)

Induction. The Naive Bayes classifiers are built on Bayesian classification methods. They rely on Bayes's theorem which is an equation describing the relationship of conditional probabilities of statistical quantities. The K-Nearest Neighbors (KNN) is a classification algorithm where the result/class of new instance is classified based on majority of K-Nearest Neighbors' category.

The Decision Tree (DT) Induction is the learning of decision trees from training set. A decision tree is a flowchart-like tree structure. The DT is a method used to partition a decision tree into smaller subsets, by partitioning or splitting the tree nodes based on a threshold value of appropriate features. The entropy is the measure of the impurity of a set of data alternatively.

The regression is used to predict a range of numeric values (also called continuous values), given a particular dataset. Regression analysis is generally categorized into two types which are simple regression (Linear) and multiple regression. The Linear Regression (LR) involves only two variables, one of which is dependent variable and the other is explanatory (independent) variable. For example, population and food production. It is represented in the form of a line:

$$\hat{y} = h_\theta(\mathbf{X}) = \boldsymbol{\theta}^T\mathbf{X} \quad (21)$$

where $\mathbf{X}$ is the input features matrix, is the parameters matrix, $\hat{y}$ is the predicted output value, and is the hypothesis. There are two types of linear regression which are Least Absolute Shrinkage and Selection Operator (Lasso) regression and Ridge regression. Lasso LR follows the regularization technique to create prediction. It is given more priority over the other regression methods because it gives an accurate prediction. Lasso regression model uses shrinkage technique. In this technique, the data values are shrunk towards a central point similar to the concept of mean. Lasso regression is taken into consideration when there are a greater number of features because it automatically performs feature selection [35]. The Ridge LR is another type of regression algorithm in data science and is usually considered when there is a high correlation between the independent variables or model parameters. As the value of correlation increases the least square estimates evaluates unbiased values. But if the collinearity in the dataset is very high, there can be some bias value. Therefore, we create a bias matrix in the equation of Ridge regression algorithm. It is a useful regression method in which the model is less susceptible to overfitting and hence the model works well even if the dataset is very small [36]. Multiple Regression has more than one independent variables. For example, home prices based on its location, square feet, price when last sold, the price of similar homes, and other factors.

B. The Proposed FSO-CC Algorithm

The block diagram of the proposed FSO-CC scheme is shown in Fig. 5. Firstly, the performance parameters of FSO communication network are specified according to the design and operation requirements. These performance parameters include the maximum transmitted power $P_T^{max}(s_{TX})$ that the FSO TX node can transmit, the maximum bit error rate $BER^{max}(s_{RX})$ at the FSO RX node, and the minimum signal to noise ratio $SNR^{min}(s_{RX})$ at the RX node.

According to the specified performance parameters and the FSO communication models, the training dataset are generated. The input features of training dataset are the distance $d(s_{TX}, s_{RX})$ and the weather conditions between the FSO TX and RX nodes, which are the rain rate $R(s_{TX}, s_{RX})$, wet snow fall rate $S_w(s_{TX}, s_{RX})$, dry snow fall rate, $S_d(s_{TX}, s_{RX})$, and the visibility $V(s_{TX}, s_{RX})$. Therefore, the number of input features for each training example is $n = 5$. The input feature matrix is defined as:

$$\mathbf{X} = [X_i^{(j)}]_{m\times(n+1)} \quad (22)$$

where $1 \le j \le m$ is the sample number which is the row number of the feature matrix, and $0 \le i \le n$ is the feature number which is the column number of the feature matrix. The dummy feature in ML models is called intercept or bias term. In practical applications, when all features are zeroes, the output has still a value. Therefore, the dummy feature prevents the model output to be a zero, when all input features are zeroes. In addition, the weight of dummy feature ensures the correct variance of the model. Therefore, it is worth to mention that the feature $X_0^{(j)} = 1$ is the dummy feature that is used to simplify the ML modelling. FSO-CC adopts the binary classification to estimate the status of FSO channel in term of suitability to use FSO communication or not. Therefore, the output label or class of ML classifier is defined to be either $suitability = 1$ for suitable FSO transmission or $suitability = 0$ for unsuitable FSO transmission. The output labels matrix of the training dataset is defined as:

$$\mathbf{y} = [\boldsymbol{y}^{(j)}]_{\boldsymbol{m\times 1}} \quad (23)$$

where $1 \le j \le m$ is the sample number which is the row number of the output labels matrix. After generating the training dataset, the ML algorithm is learned as shown in Fig. 5 to build the model between the input and output through getting the hypothesis $h_\theta(X)$ where θ is the ML parameters. For any new input features which are the distance and weather conditions between FSO TX and RX nodes, the learnt ML model can predict the output class which is the channel estimation of FSO transmission suitability.

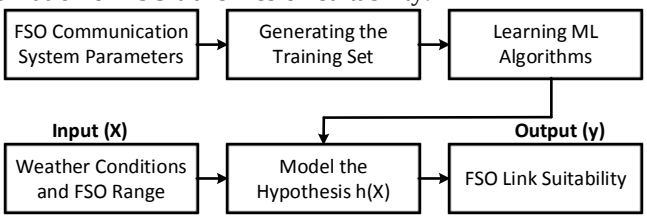

Fig. 5. Block Diagram of FSO-CC Algorithms

In Algorithm 1, the dataset is generated to learn the ML algorithms. In Line 1, the FSO performance parameters including $P_T^{max}(s_{TX})$, $BER^{max}(s_{RX})$, and $SNR^{min}(s_{RX})$ are stated. In Line 2, the parameters of TX, RX, and FSO signal are stated according to the hardware equipment at TX and RX such as the FSO frequency, the TX and RX antennas specifications, photodiode sensitivity, and others. The values of all these parameters are stated in Section 6. The training example number is initialized in Line 3. From Line 4 to line

18, the m training examples are randomly generated. The input features $X_i^{(j)}$ is randomly generated in Line 5. According to the generated input features $X_i^{(j)}$, the geometric loss, the atmospheric losses of rain, snow, and fog, and the total losses are calculated from Line 6 to Line 10 using the equations of the FSO communication models. The minimum received power $P_R^{min}(s_{RX})$ and the minimum transmitted power $P_T^{min}(s_{TX})$ that are required to satisfy the FSO performance parameters are computed in Line 11 and 12 using the equations of the FSO communication models. From Line 13 to Line 16, the value of the output class $y^{(j)}$ of suitability is determined according to the comparing the values of $P_T^{min}(s_{TX})$ and $P_T^{max}(s_{TX})$. The training example number is incremented in Line 18 to create new training example. Algorithm 1 is executed one time to generate the dataset. If the parameters of FSO performance or TX, RX, and FSO signal are changed, Algorithm 1 is required to be executed to update the training dataset.

Algorithm 1: FSO-CC Dataset Generation Algorithm

1. **Specify:** The FSO performance parameters
2. **Specify:** The TX/RX/FSO parameters
3. **Set:** $j = 1$
4. **Repeat:**
5. **Training Example *j***: Generate random input features $X_i^{(j)}$of rain rate $X_1^{(j)}$, snow rate $X_2^{(j)}$, visibility $X_3^{(j)}$, and the distances $X_4^{(j)}$, and store features in **X**
6. **Calculate:** The geometric losses using Equation (1);
7. **Calculate:** The fog losses using Equation (2);
8. **Calculate:** The rain losses using Equation (5);
9. **Calculate:** The snow losses using Equation (6);
10. **Get:** The total losses $L_{AT}(s_{TX}, s_{RX})$ using Equation (18);
11. **Compute:** The minimum received power $P_R^{min}(s_{RX})$ that satisfies the FSO performance parameters by solving Equation (12) and (19)
12. **Compute:** The minimum transmitted power $P_T^{min}(s_{TX})$ that satisfies the FSO performance parameters by solving Equation (13)
13. **if** $[P_T^{min}(s_{TX}) \leq P_T^{max}(s_{TX})]$:
14. **Set:** The output class of suitability is one $y^{(j)} = 1$
15. **else:**
16. **Set:** The output class of suitability is zero $y^{(j)} = 0$
17. Store: the output class $y^{(j)}$ in **y**
18. $j = j + 1$
19. **Until** $\boldsymbol{j == m}$

Algorithm 2 shows the ML classification algorithms for the proposed FSO-CC scheme. In Line 1, the training dataset that is generated using Algorithm 1 is imported. The dataset is scaled in Line 2 using standardization. The standardization is performed by subtracting the average value of each feature from the feature value and dividing the result to the feature standard deviation as follows:

$$\tilde{\boldsymbol{X}}_{\boldsymbol{i}}^{(\boldsymbol{j})} = \frac{\boldsymbol{X}_{\boldsymbol{i}}^{(\boldsymbol{j})} - \boldsymbol{\mu_i}}{\boldsymbol{\sigma_i}} \quad (24)$$

where $0 \leq i \leq n$, and μ_i and σ_i are features average and standard deviation values, respectively which are computed as follows:

$$\boldsymbol{\mu_i} = \frac{\boldsymbol{1}}{\boldsymbol{m}} \sum_{\boldsymbol{k=1}}^{\boldsymbol{m}} \boldsymbol{X}_{\boldsymbol{i}}^{(\boldsymbol{k})} \quad (25)$$

$$\boldsymbol{\sigma_i} = \sqrt{\frac{\sum_{\boldsymbol{k=1}}^{\boldsymbol{m}} (\boldsymbol{X}_{\boldsymbol{i}}^{(\boldsymbol{k})} - \boldsymbol{\mu_i})^{\boldsymbol{2}}}{\boldsymbol{m}}} \quad (26)$$

In Line 3, the training dataset is split into 30% of testing examples and 70% of training examples. In Line 4, the parameters of ML algorithms are tuned using k-fold cross-validation to get its optimal values [37]. In this paper, the Logistic Regression (LR), Random Forest (RF), Support Vector Machine (SVM), and Decision Tree (DT) classification algorithms are used to estimate the FSO channel [38] and [39]. In case of using LR classifier, the parameters such as the error plenty λ and the regularization type are tuned to get the optimal λ and the best regularization type that maximize the classification accuracy. In DT classifier, the maximum depth of DT and the criterion function to evaluate the split.

The ML classifiers are learnt using the training examples in Line 5. In LR classifier, the regularization is performed by adding a plenty term in the cost function to overcome the overdraft and high variance of the training ML model. The logistic regression that adopts L2 norm for regularization is called Ridge logistic regression. The cost function of Ridge logistic regression is given by [36]:

$$J(\theta) = -\frac{1}{m}\sum_{i=1}^{m}\{y^{(i)} log\left[h_\theta\left(X^{(i)}\right)\right] + \left(1 - y^{(i)}\right) log\left[1 - h_\theta\left(X^{(i)}\right)\right]\} + \frac{\lambda}{2m}\sum_{j=1}^{n}\theta_j^2 \quad (27)$$

where λ is the plenty of the error which is used in regularization and θ are the parameters of logistic regression that are computed when the logistic regression algorithm is trained. The logistic regression that adopts L1 norm for regularization is called Lasso logistic regression. The cost function of Lasso logistic regression is given by [35]:

$$J(\theta) = -\frac{1}{m}\sum_{i=1}^{m}\{y^{(i)} log\left[h_\theta\left(X^{(i)}\right)\right] + \left(1 - y^{(i)}\right) log\left[1 - h_\theta\left(X^{(i)}\right)\right]\} + \frac{\lambda}{m}\sum_{j=1}^{n}\theta_j \quad (28)$$

In DT classifier, the criterion functions to evaluate the split is either the cross-entropy loss (EL) or the Gini loss (GL) [40]. EL and GL the disorder or uncertainty of a group. The cross entropy lies between 0 to 1 and it measures the impurity of split according to the following formula:

$$EL = \sum_c -\hat{p}_c log_2(\hat{p}_c) \quad (29)$$

where c is class label and $\hat{p}_c$ is the proportional of c class. On the other hand, GL has computational power compared with EL. The GL lies between 0 to 0.5, and the impurity in the GL is calculated as [41]:

$$GL = \sum_c \hat{p}_c(1 - \hat{p}_c) = 1 - \sum_c(\hat{p}_c)^2 \quad (30)$$

The split with highest Information Gain (IG) is selected where IG is computed as follows:

$$IG(R) = H(R) - \sum_i w_i\, H(S_i) \quad (31)$$

$$w_i = \frac{|S_i|}{|R|} \quad (32)$$

where R is the parent/root node, S_i is the i^{th} child node, H

is the EL or GL, w_i is the weight which is the relative size of the i^{th} child node with respect to the parent node, $|S_i|$ is the number of examples in the of i^{th} child node, and $|R|$ is the number of examples in the of the root node.

In Line 6, the train score accuracy of trained features and labels or classes is obtained. In line 7, the ML algorithm predicts the values of output labels **y**_$pred$ for the test input features **X**_$test$. In Line 8, the performance metrics of the ML classifiers including confusion matrix, accuracy score, specificity, sensitivity, and F1 score are evaluated. The code from Line 9 to Line 18 is repeated and executed when the FSO node requires a transmission of new data. When the communication activity is needed in the FSO node, the new input features **X**_new that consists from the current weather conditions and communication distance are firstly obtained. Then, the ML classifier predicts the output class y_new of suitability which indicates the status of FSO channel. From Line 13 to 16, the communication links are selected based on the features inputs (i.e. weather conditions and distance between nodes). The suitability value of one indicates that the weather conditions does affect the FSO link between the two nodes. Conversely, the suitability value of zero means that the weather conditions hardly affects the FSO link between the two nodes. Therefore, FSO direct communication is performed when the suitability equals to one. Otherwise, any other communication methods such as indirect FSO links (i.e. multi-path FSO links that satisfies the performance requirements) or other direct communications systems are used.

Algorithm 2: FSO-CC Classification Algorithm

1. **Import:** The generated dataset (**X**, **y**)
2. **Standardization:** Standard scalar for generated examples
3. **Split:** The generated examples are split into 70% training examples (**X**_$train$, **y**_$train$) and 30% testing examples (**X**_$test$, **y**_$test$)
4. **Tuning:** get the optimal parameters of ML algorithms
5. **Fit:** The ML algorithm is trained using (**X**_$train$, **y**_$train$)
6. **Score:** Get the train score of the ML model **X**_$train$, **y**_$train$
7. **Predict:** Estimate the output labels **y**_$pred$ for **X**_$test$ input
8. **Metrics:** Evaluate the performance metrics of classifier using (**y**_$test$, **y**_$pred$)
9. **while (true):**
10. **if** (Communication is required):
11. **Get:** The new input features **X**_new
12. **Predict:** the output class of suitability y_new
13. **if** ($suitability = 1$):
14. **FSO Communication:** Transmit using FSO Direct Link
15. **else:**
16. **Others Communication Methods:** Look for available indirect FSO Links, or other communication systems
17. **end if**
18. **end while**

VI. Results and Discussion

A. Simulation Assumptions

In this section, the performance of the proposed FSO-CC scheme is evaluated by modelling and simulating its algorithms and functions. Python 3 is used to build the simulation environment using an Intel Core i7 2.7 GHz processor and 24GB memory. Unless it is clearly stated, Table 1 states the parameters assumptions used in the simulation environment [42], [28], and [43].

TABLE 1
The Simulation Assumptions

Parameter	Symbol	Value	Unit
FSO wavelength	λ	1550	nm
FSO frequency	f	193.5	THz
TX aperture diameter	$D_T(s_{TX})$	4	cm
RX aperture diameters	$D_R(s_{RX})$	20	cm
System bandwidth	BW	1	GHz
System losses	$L_{sys}(s_{TX}, s_{RX})$	0.5	-
divergence angle	$\theta(s_{TX}, s_{RX})$	2	mm.rad /m
Electronic charge	q	1.602×10^{-19}	C
Multiplication gain	G_i	10	-
Excess noise factor	$F(G_i)$	3.2	-
Photodiode sensitivity	$s(s_{RX})$	0.9	A/W
Boltzmann constant	k	1.38×10^{-25}	J/K
Resistance of the amplifier	$R_{load}(s_{RX})$	50	Ω
Absolute temperature	$Temp$	298	K
Minimum SNR	$SNR^{min}(s_{TX}, s_{RX})$	15.56	dB
Maximum of transmitted power	$P_T^{max}(s_{TX})$	0	dBm
Maximum BER	$BER^{max}(s_{TX}, s_{RX})$	10^{-10}	-
Number of training examples	m	1596	-

The plenty of error in Logistic Regression	λ	0.01	-
Logistic Regression Regularization	-	Lasso	-
The maximum depth of DT classifier	-	20	-
k-fold cross-validation	k	10	-

In this paper, a real weather conditions in Gaza Strip/Palatine are considered to predict the FSO communication availability.

World weather online [44] provides up to date and accurate weather information and forecasting worldwide. Four millions cities/towns are covered by world weather online. Many organizations use and trust world weather online such as Weathercare, kydive Mag, G&D Creations, and Surfcast. Therefore, a dataset for weather forecasting in Gaza Strip is obtained from January, 2009 to June, 2022 in monthly basis [44]. The latitude and longitude of the weather measurements are 31.4978 and 34.4684, respectively which is the Gaza Strip area. The number of examples in the dataset is 162. The dataset contains 29 features related to the weather conditions. Firstly, the data is understood. Fig. 6 describes the data.

```
       loc_id        year       month    maxtempC    maxtempF    mintempC  \
count   162.0  162.000000  162.000000  162.000000  162.000000  162.000000
mean      1.0 2015.259259    6.388889   24.716049   76.401235   19.524691
std       0.0    3.914546    3.460962    4.640450    8.300610    4.694652
min       1.0 2009.000000    1.000000   15.000000   60.000000   12.000000
25%       1.0 2012.000000    3.000000   21.000000   69.000000   15.000000
50%       1.0 2015.000000    6.000000   25.000000   77.500000   20.000000
75%       1.0 2019.000000    9.000000   29.000000   84.000000   24.000000
max       1.0 2022.000000   12.000000   32.000000   89.000000   27.000000

       mintempF    avgtempC    avgtempF      rainMM  ...  avgwindgustKmph  \
count  162.000000  162.000000  162.000000  162.000000  ...       162.000000
mean    67.160494   23.000000   73.395062   41.252716  ...        18.833951
std      8.492535    4.774414    8.508934   59.115650  ...         3.794245
min     53.000000   14.000000   58.000000    0.000000  ...        12.600000
25%     59.250000   18.000000   65.000000    1.000000  ...        16.025000
50%     67.500000   23.500000   74.000000   13.050000  ...        17.800000
75%     75.000000   27.000000   81.000000   62.975000  ...        21.750000
max     81.000000   30.000000   87.000000  313.300000  ...        28.300000

       visibilityKm  visibilityMiles    humidity   pressureMB  pressureInches  \
count    162.000000       162.000000  162.000000   162.000000      162.000000
mean       9.962963         5.888889   62.790123  1013.711728       30.411111
std        0.189438         0.315244    4.988723     3.773879        0.119002
min        9.000000         5.000000   48.000000  1005.800000       30.200000
25%       10.000000         6.000000   60.000000  1011.000000       30.300000
50%       10.000000         6.000000   62.000000  1013.900000       30.400000
75%       10.000000         6.000000   66.000000  1016.700000       30.500000
max       10.000000         6.000000   76.000000  1021.500000       30.600000

       cloudcover    sun_hour    sun_days     uvindex
count  162.000000  162.000000  162.000000  162.000000
mean    14.765432  352.438272   28.604938    5.783951
std     10.548052   24.206139    2.798309    1.307974
min      1.000000  261.000000   18.000000    3.000000
25%      7.000000  344.250000   27.250000    5.000000
50%     12.000000  360.000000   30.000000    6.000000
75%     20.750000  371.000000   31.000000    7.000000
max     52.000000  372.000000   31.000000    8.000000

[8 rows x 29 columns]
```

Fig. 6. Dataset Description

After that the data cleaning is performed. The irrelevant features are removed. Feature selection is performed to remove the duplicated and irrelevant features. The weather conditions features related to the FSO channel are selected which include rain rate in mm/h, snow fall rate in mm/h, temperature in degree Celsius, and visibility in km. Fig. 7 shows the selected features information.

```
<class 'pandas.core.frame.DataFrame'>
RangeIndex: 162 entries, 0 to 161
Data columns (total 6 columns):
 #   Column        Non-Null Count  Dtype
---  ------        --------------  -----
 0   year          162 non-null    int64
 1   month         162 non-null    int64
 2   avgtempC      162 non-null    int64
 3   rainMM        162 non-null    float64
 4   snow_cm       162 non-null    int64
 5   visibilityKm  162 non-null    int64
dtypes: float64(1), int64(5)
memory usage: 7.7 KB
```

Fig. 7. Dataset Information

The missing data is checked and handled. The correlation heat map is shown in Fig. 8.

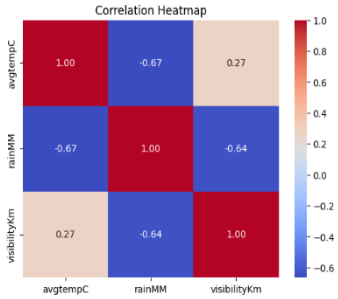

Fig. 8. Correlation among Features

Furthermore, the FSO nodes that connected to each other are considered as a set of real and popular educational, Internet Service Provider (ISP), and highest buildings places in Gaza Strip. Table 2 shows the names and the considered identifications (ID) of the suggested twelve places. Additionally, Fig. 9 shows the locations of these places on the map [45].

TABLE 2
THE NAME AND IDS OF STUDIED FSO NODES

FSO Node Name	FSO Node ID
Islamic University of Gaza	1
Al Azhar University of Gaza	2
Al Aqsa University	3
Speedclick ISP company	4
Al Ghafry Tower	5
Bank of Palestine Tower	6
Susi Tower	7
Al Zafer 9 Tower	8
Dawood Tower	9
Al Watan Tower	10
Fusion ISP company	11
PalTel ISP company	12

Fig. 9. The locations of studied FSO nodes in the map [45]

B. Simulation Results

Since the distance is one of the important parameters in FSO communications that affects the quality of communication links, the distance between each FSO nodes and all other FSO nodes are calculated, analyzed and tabulated in Fig. 10. Therefore, FSO ranges are used to refer to these distances. The twelve studied FSO nodes are shown by IDs is Fig. 10. The distances are range from 0 km and 1.9 km.

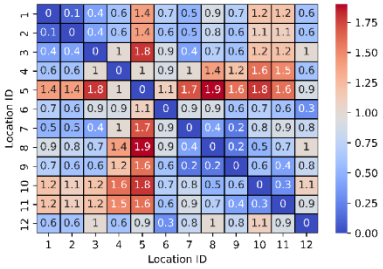

Fig. 10. FSO Range (Km) among the studied FSO nodes

The dataset related to the weather conditions in the Gaza Strip is obtained through the world weather website [44]. The weather conditions collected for Gaza Strip are rain rate (mm/h), visibility (km), and snow rate(mm/h). The weather conditions readings are monthly averaged in the interval from January, 2009 to June, 2022. In Fig. 11 shows the monthly averaged values for rate, visibility, and snow rate. As shown in Fig. 11, it is worth to mention that the most affected weather factor of FSO communication in Gaza strip is the rain.

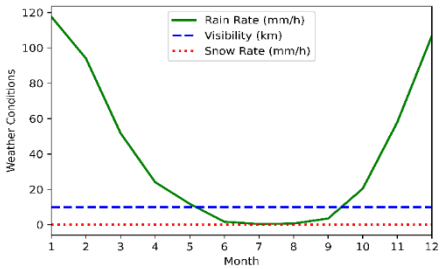

Fig. 11. The Monthly Averaged Weather Conditions in Gaza Strip

The weather conditions indication $WCI(s_{TX}, s_{RX})$ is used in Fig. 12 to reflect the effect of weather conditions. Therefore, it is computed as follows:

$$WCI(s_{TX}, s_{RX}) = R^{\alpha}(s_{TX}, s_{RX}) + S^{b}(s_{TX}, s_{RX}) + \frac{1}{V(s_{TX}, s_{RX})} \quad (33)$$

Therefore, the input features are shorted to two features which are $WCI(s_{TX}, s_{RX})$ and $d(s_{TX}, s_{RX})$. By analyzing and mining the dataset, the suitability status of channel **y** for the first 400 training examples is plotted in Fig. 12 for every coordination point of the weather conditions indication $WCI(s_{TX}, s_{RX})$ and the distance $d(s_{TX}, s_{RX})$ between the TX and RX nodes. It is noted that the class of suitability is zero for high values of $WCI(s_{TX}, s_{RX})$ and high values of $d(s_{TX}, s_{RX})$. This is because the received FSO signal does not satisfy the performance parameters for bad weather conditions or high separate distance between the FSO TX and RX nodes.

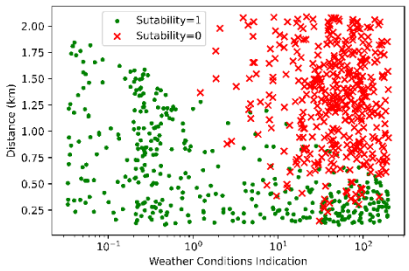

Fig. 12. The Suitability Classes for Distance and Weather Conditions Indication

Fig. 13 shows classification accuracy of the LR classifier versus the plenty of the error λ for Lasso and Ridge LR. The classification accuracy is affected by the values of λ as shown in Fig. 13. With increasing the λ values for Lasso regression, the accuracy is increasing at the beginning and then it starts decreasing until the accuracy reaches to a constant value. On the other hand, the accuracy in Ridge LR increases at low λ value and starts decreasing gradually with the increase of the λ value. The highest value of classification accuracy occurs when using Lasso regression at $\lambda = 0.01$. Therefore, Lasso LR with $\lambda = 0.01$ is used to be trained and modeled using the dataset.

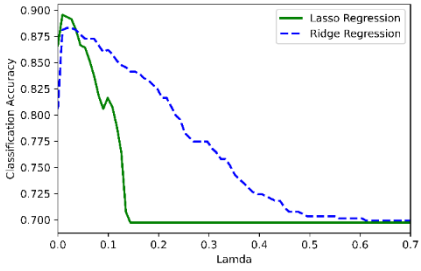

Fig. 13. Classification accuracy versus the plenty of the error for LR classifier.

In Fig. 14, the classification accuracy versus the maximum depth of DT classifier for GL and EL criterions are plotted. At the beginning, the classification accuracy increases with increasing the maximum depth of DT classifier. After that, the classification accuracy remains fixed with increasing the maximum depth of DT classifier. The results in the Fig. 14 show that the EL criterion is better in term of the classification accuracy. Therefore, EL criterion DT classifier with maximum depth of 20 is used to be trained and modeled using the generated dataset.

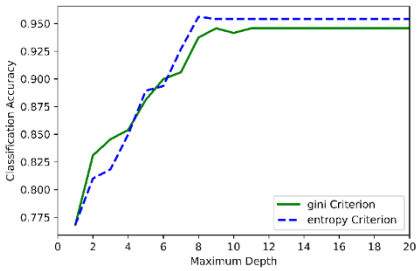

Fig. 14. Classification Accuracy versus the Maximum Tree Depth for DT Classifier

After generating, mining, and processing the dataset, and building the ML model, the performance metrics of ML classifiers are evaluated using confusion matrix, accuracy, specificity, sensitivity and F1 score. The confusion matrix shows the number of examples that correctly and incorrectly predicted. In Fig. 14, the confusion matrices of the LR, SVM, and RF classifiers are shown. The first row at the bottom of the confusion matrix shows the number of examples that correctly (i.e. True Positive (TP)) and incorrectly (i.e. False Negative (FN)) predicted as suitable examples for FSO communication. On the other hand, the second row at the top of the confusion matrix shows the number of examples that incorrectly (i.e. False Positive (FP)) and correctly (i.e. True Negative (TN)) predicted as unsuitable for FSO communication. The performance of ML classifier increases for high number of TP and TN examples, which are the summation of the first diagonal of the confusion matrix. Similarly, it rises for low number of FP and FN examples, which are the summation of the second diagonal of the confusion matrix. Therefore, the rows and columns of confusion matrix represent the actual and predicted labels, respectively. As shown in Fig. 15, the SVM classifier is better in term of prediction errors between the real values and the predictive values of examples.

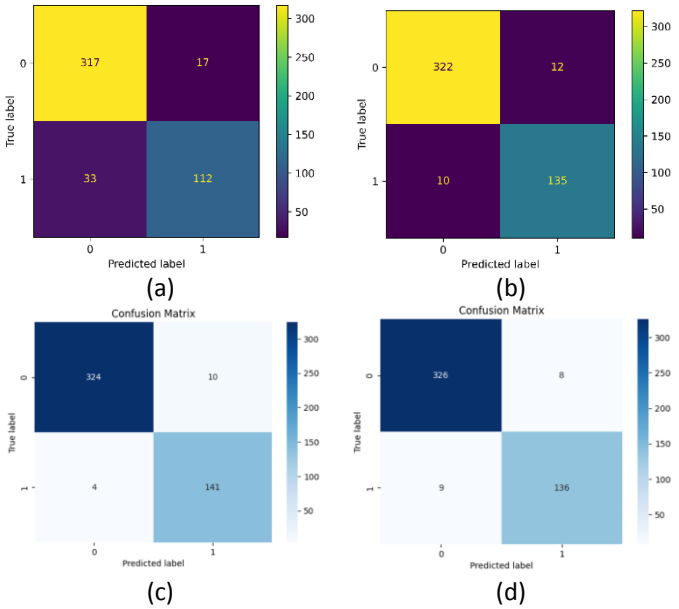

Fig. 15. Confusion Matrix: (a) LR Classifier, (b) DT Classifier, (c) SVM, and (d) RF

In the Table 3, the accuracy score, train and test score, specificity, sensitivity and F1 Score are shown for LR and DT classifiers. The accuracy score is the percentage of corrected prediction of examples (i.e. TP+TN) with respect to all examples (i.e. TP+TN+FP+FN) and it is computed as follows:

$$Accuracy\ Score = \frac{TP+TN}{TP+TN+FP+FN} \quad (34)$$

The sensitivity or the recall score is the percentage of corrected prediction of positive examples (i.e. TP) with respect to all examples that are predicted as positive examples (i.e. TP + FN). It is computed as follows:

$$Sensitivity\ = \frac{TP}{TP+FN} \quad (35)$$

The specificity or the precision score is the percentage of corrected prediction of positive examples (i.e. TP) with respect to all actual positive examples (i.e. TP + FP). It is computed as follows:

$$Specificity\ = \frac{TP}{TP+FP} \quad (36)$$

The F1 score combines the recall score and the precision score, and it is computed as follows:

$$F1\ Score\ = 2 \times \frac{Sensitivity \times Specificity}{Sensitivity + Specificity} \quad (37)$$

The train and test scores evaluate the fitting of ML classifier using the training and testing examples. As shown in Table 3, the accuracy score of DT is 0.95 which means that 95% of test examples are predicted correctly and 5% are predicted incorrectly. Similarly, the accuracy score of LR, SVM, and RF are is 0.90, 0.97, and 0.96, respectively.

The sensitivity or the recall score of DT is 0.95 which means that 95% of test examples that actually labeled as "suitable" are predicted correctly and 5% are predicted incorrectly. Similarly, the sensitivity or the recall score of LR, SVM, and RF are is 0.90, 0.97, and 0.96, respectively.

The specificity or the precision score of DT is 0.95 which means that 95% of examples that are classified as "suitable" are predicted correctly and 5% are predicted incorrectly. Similarly, the specificity or the precision score of LR, SVM, and RF are is 0.90, 0.97, and 0.96, respectively.

The F1 score balances the precision and recall. The F1 score of DT, LR, SVM, and RF are 0.95, 0.90, 0.97, and 0.96, respectively. This indicates that both precision and recall are high and the ML models are performed well.

Therefore, SVM classifier is better in term of metrics performance, compared other classifiers. Therefore, SVM classifier is used to predict the output label of suitability for any new input data of weather conditions and distance between TX and RX FSO nodes.

TABLE 3
PERFORMANCE METRIC FOR DT AND LR CLASSIFIERS

Metric Value	ML Classifier			
	DT	LR	SVM	RF
Accuracy Score	0.95	0.90	0.97	0.96
Recall Score (Sensitivity)	0.95	0.90	0.97	0.96
Precision Score (Specificity)	0.95	0.90	0.97	0.96

F1 Score	0.95	0.90	0.97	0.96

Fig. 16 shows the predicted class of the suitability between different FSO nodes, for the monthly average weather conditions in Gaza Strip that are plotted in Fig. 11, and the distances between FSO and RX nodes that are plotted in Fig. 10. The results show that when the environmental weather conditions are bad, the FSO communication is less effective and weakens. Furthermore, the FSO communication is not possible for high distance separation between FSO nodes. As shown in Fig. 16, the FSO communication is more effective in summer and spring seasons in Gaza Strip, compare with the winter and autumn seasons because of the rain fall in winter and autumn seasons. Therefore, the proposed FSO-CC scheme is a Decision Support System (DSS) that decide if it is possible to transmit the data using FSO or other communication links according to the current weather conditions and distance between the FSO TX and RX nodes.

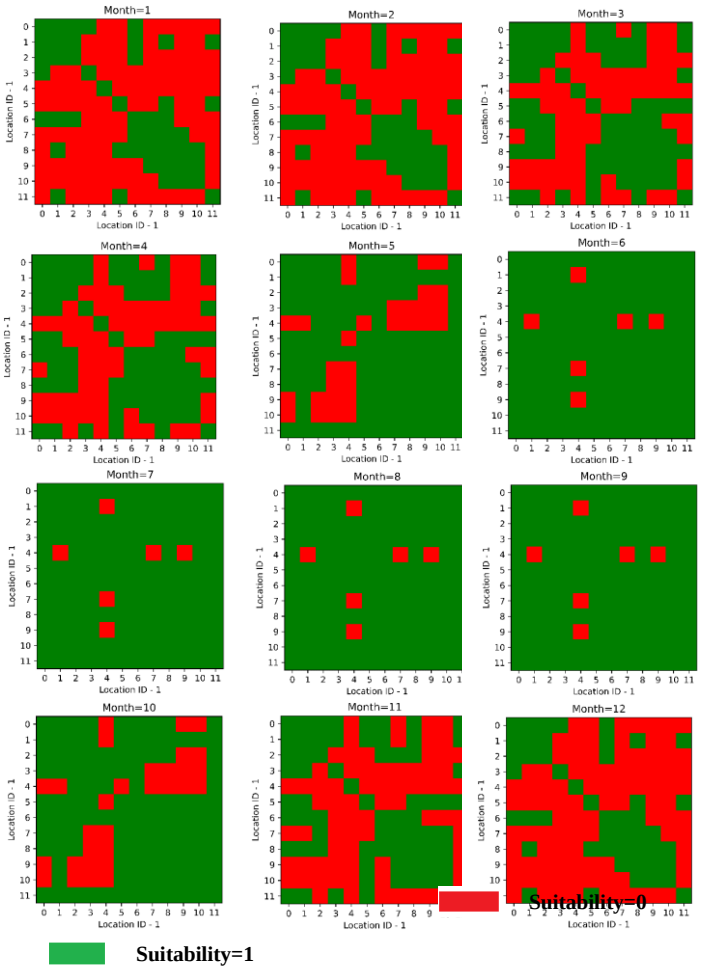

Fig. 16. Classified Suitability among the FSO Nodes for all Month

Fig. 17 and Fig. 18 show the number of occurrences for $suitability = 0$ and $suitability = 1$ with changing $SNR^{min}(s_{TX}, s_{RX})$ for $P_T^{max}(s_{TX}) = 0$ dBm and $P_T^{max}(s_{TX})$ for $SNR^{min}(s_{TX}, s_{RX}) = 15.56\,dB$, respectively. $SNR^{min}(s_{TX}, s_{RX})$ changes from 5 dB to 50 dB with 5 dB steps and $P_T^{max}(s_{TX})$ changes from -20 dBm to 25 dBm with 5 dBm steps.

For each value of $SNR^{min}(s_{TX}, s_{RX})$, the training dataset is generated using Algorithm 1. Then, the generated training dataset is used to learn the DT classifier to get the model of DT classifier for prediction using Algorithm 2. After that, the monthly weather conditions in Gaza Strip during a whole year and each possible distance between the FSO TX and RX nodes are passed as a new input features $\mathbf{X}\_new$ to DT classifier to predict the output label of suitability y_new. Therefore, $\mathbf{X}\_new$ has $12\,months \times 12\,FSO\,nodes \times 12\,FSO\,nodes = 1728$ inputs to DT classifier, which are predicted to get 1728 suitability outputs values. The same steps are performed for each value of $P_T^{max}(s_{TX})$.

The number of occurrences of when $suitability = 0$ and $suitability = 1$ are recorded and plotted in Fig. 14 and Fig. 15 for each value of $SNR^{min}(s_{TX}, s_{RX})$ and $P_T^{max}(s_{TX})$, respectively. With increasing the $SNR^{min}(s_{TX}, s_{RX})$, the transmitted power that is required to satisfy $SNR^{min}(s_{TX}, s_{RX})$ increases. Since the $P_T^{max}(s_{TX})$ of the FSO TX node is fixed to 0 dBm, the number of occurrences for $suitability = 0$ rises as shown in Fig. 17. With increasing the $P_T^{max}(s_{TX})$, the chance to increase the transmitted power that is required to satisfy $SNR^{min}(s_{TX}, s_{RX})$ increases. Therefore, the number of occurrences for $suitability = 1$ rises as shown in Fig. 18.

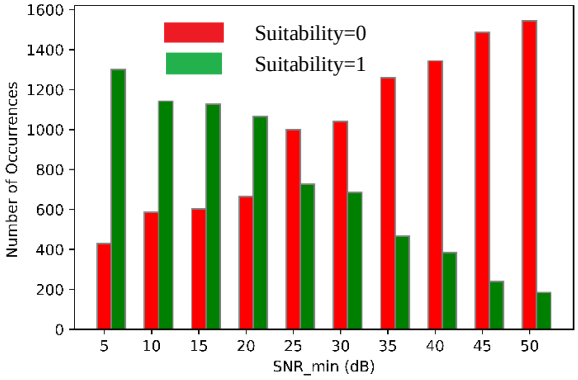

Fig. 17. The number of occurrences versus $SNR^{min}(s_{TX}, s_{RX})$ for different suitability values

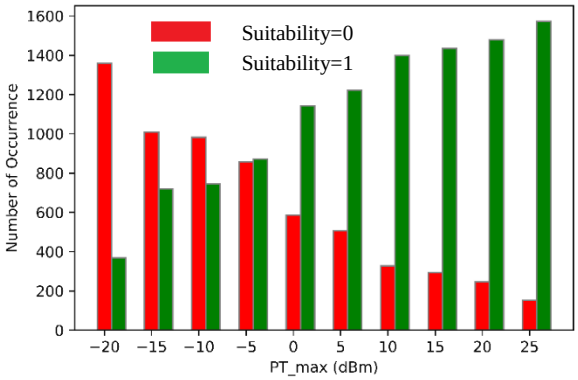

Fig. 18. The number of occurrences versus $P_T^{max}(s_{TX})$ for different suitability values

In Fig. 19 and Fig. 20, the number of occurrences for

$suitability = 1$ and $suitability = 0$ are plotted with the $P_T^{max}(s_{TX})$ for different values of $SNR^{min}(s_{TX}, s_{RX})$, respectively. The dataset for any new FSO performance such as $SNR^{min}(s_{TX}, s_{RX})$ and FSO TX node capabilities such as $P_T^{max}(s_{TX})$ is generated using Algorithm 1. After that, the DT classifier is trained and modeled using Algorithm 2. As it is discussed in Fig. 18, with increasing $P_T^{max}(s_{TX})$, the number of occurrences for $suitability = 1$ increases as shown in Fig. 19, and the number of occurrences for $suitability = 0$ decreases as shown in Fig. 20. As it is discussed in Fig. 17, with increasing $SNR^{min}(s_{TX}, s_{RX})$, the number of occurrences for $suitability = 1$ decreases as shown in Fig. 19, and the number of occurrences for $suitability = 0$ rises as shown in Fig. 20. Therefore, the FSO communication is more efficient and available when increasing the FSO TX parameters such as increasing its capability of transmitting high power. Furthermore, reducing of the FSO performance in term of minimum received SNR leads to enhance the suitability of using FSO communication.

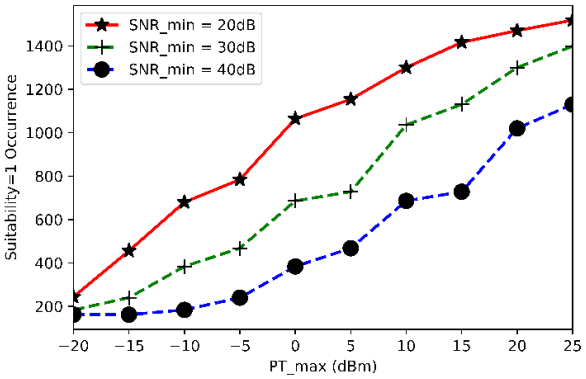

Fig. 19. The number of occurrences of $suitability = 1$ with $P_T^{max}(s_{TX})$ for different $SNR^{min}(s_{TX}, s_{RX})$

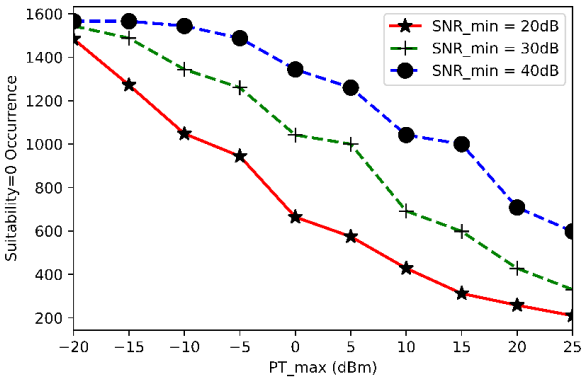

Fig. 20. The number of occurrences of $suitability = 0$ with $P_T^{max}(s_{TX})$ for different $SNR^{min}(s_{TX}, s_{RX})$

VII. Conclusions

This paper emphasizes on the Free Space Optical (FSO) as a communication link between different locations on the ground for secure and high data transfer. Real time weather data including rain, visibility, and snow is obtained for Gaza Strip and is averaged for a period of twelve months. Furthermore, the distances among different actual locations in Gaza Strip is computed and tabulated. Decision tree and logistic regression classifiers are adopted to predict the channel suitability. The training dataset is generated to train the machine learning classifiers, according to the weather data, FSO transmitter and receiver parameters, and the distances among locations. The weather data and distances among locations are used as input features for machine learning classifiers. The output label of the machine learning classifiers is the class of channel suitability for FSO communication which is either a value of zero for channel stability and a value of one for channel unsuitability. The results show that in the presence of bad environmental factors, the quality of FSO channel is not suitable for FSO communication. Moreover, with increasing the transmitted power or reducing the required minim signal to noise ratio, the FSO channel stability improves. The performance of the decision tree and logistic regression classifiers are compared, and the results show that the decision tree classifier has better accuracy, sensitivity and fewer errors between the true and predictive values, compared with decision tree classifier.

The future work focuses in developing a routing algorithm to find the best multi-path route (i.e. indirect path) between the FSO TX and RX nodes, once the direct FSO path between FSO TX and RX nodes is unsuitable for FSO communication.

References

[1] Maswikaneng, S.P., et al. Atmospheric effects on free space optics wireless communication: applications and challenges. in 2018 International Conference on Intelligent and Innovative Computing Applications (ICONIC). 2018. IEEE.

[2] Global Market Insights "Free Space Optics (FSO) Communication Market Size By Platform (Terrestrial, Satellite, Airborne), By Application (Mobile Backhaul, Enterprise Connectivity, Disaster Recovery, Defense, Satellite), COVID-19 Impact Analysis, Regional Outlook, Growth Potential, Competitive Market Share & Forecast, 2021 – 2027", Global Market Insights, November 2021.

[3] Yang, Z., Gu, R., Dong, T., Yin, J., Li, S., Liu, Z., ... & Ji, Y. (2018, October). An artificial neural network-based attenuation tomography in free space optical network. In 2018 International Conference on Networking and Network Applications (NaNA) (pp. 52-57). IEEE.

[4] Arun K. Majumdar, in Optical Wireless Communications for Broadband Global Internet Connectivity, 2019

[5] Ifrah G. The universal history of computing: from the abacus to the quantum computer. New York: John Wiley; 2001.

[6] Hu, J., Niu, H., Carrasco, J., Lennox, B., & Arvin, F. (2020). Voronoi-based multi-robot autonomous exploration in unknown environments via deep reinforcement learning. IEEE Transactions on Vehicular Technology, 69(12), 14413-14423.

[7] Mahammad, Y., & Bakirova, L. Machine Learning Concepts and Applications.

[8] Kargupta H. Next generation of data mining. Boca Raton: CRC Press; 2009.

[9] El Naqa, Issam, and Martin J. Murphy, "What is machine learning? In machine learning in radiation oncology." Springer, Cham., 2015.

[10] Alpaydin E. Introduction to machine learning. 3rd ed. Cambridge, MA: The MIT Press; 2014.

[11] Bishop, C. M., & Nasrabadi, N. M. (2006). Pattern recognition and machine learning (Vol. 4, No. 4, p. 738). New York: springer.

[12] Esmail, M. A., Saif, W. S., Ragheb, A. M., & Alshebeili, S. A. (2021). Free space optic channel monitoring using machine learning. Optics Express, 29(7), 10967-10981.

[13] M. A. Khalighi and M. Uysal, “Survey on free space optical communication: A communication theory perspective,” IEEE Commun. Surv. Tutorials 16(4), 2231–2258 (2014).
[14] Vitásek, J., et al. Atmospheric turbulences in free space optics channel. in 2011 34th International Conference on Telecommunications and Signal Processing (TSP). 2011. IEEE.
[15] Tabassum, N., et al. Performance analysis of free space optics link for different cloud conditions. in 2018 4th International Conference on Computing Communication and Automation (ICCCA). 2018. IEEE.
[16] Kiran, K. V., Perinbaraj, S., Pradhan, J., Mallick, P. K., Turuk, A. K., & Das, S. K. (2020). Machine learning aided switching scheme for hybrid FSO/RF transmission. Intelligent Decision Technologies, 14(4), 529-536.
[17] Priyanshu Mishra, Sonali, Abhishek Dixit, Virander Kumar Jain. (2020). Machine Learning Techniques for Channel Estimation in Free Space Optical Communication Systems.
[18] Ragheb, A., Saif, W., Trichili, A., Ashry, I., Esmail, M. A., Altamimi, M., ... & Alshebeili, S. (2020). Identifying structured light modes in a desert environment using machine learning algorithms. Optics Express, 28(7), 9753-9763.
[19] S. A. Al-Gailani et al., "A Survey of Free Space Optics (FSO) Communication Systems, Links, and Networks," in IEEE Access, vol. 9, pp. 7353-7373, 2021, doi: 10.1109/ACCESS.2020.3048049.
[20] Kim, Issac I. and Eric Korevaar. Availability of Free Space Optics (FSO) and Hybrid FSO/RF Systems. Optical Access, Incorporated; 2002.
[21] S. Bloom, E. Korevaar, J. Schuster, H. Willebrand Understanding the performance of free-space optics J Opt Network, 2 (2003), pp. 178-200.
[22] Alkholidi, Abdulsalam Ghalib, and Khaleel Saeed Altowij. "Free space optical communications—theory and practices." Contemporary Issues in Wireless Communications (2014): 159-212.
[23] Kim II, McArthur B, Korevaar E. Comparison of laser beam propagation at 785 nm and 1550 nm in fog and haze for optical wireless communications. In: SPIE photonics east/optical wireless communications III; 2000, p. 26–37.
[24] Achour M.. Simulating Atmospheric Free-Space Optical Propagation part I, Haze, Fog and Low Clouds, Rainfall Attenuation. Optical Wireless Communications. Proceedings of SPIE; 2002.
[25] “Prediction methods required for the design of terrestrial free-space optical links,” ITU-R Recommendation P.1814, 2007.
[26] J. M. Kahn and J. R. Barry, “Wireless infrared communications,” Proceedings of the IEEE, vol. 85, no. 2, pp. 265–298, 1997.
[27] Xu, F., Khalighi, M. A., & Bourennane, S. (2011, June). Impact of different noise sources on the performance of PIN-and APD-based FSO receivers. In Proceedings of the 11th International Conference on Telecommunications (pp. 211-218). IEEE.
[28] Kaymak, Yagiz, Sina Fathi-Kazerooni, Roberto Rojas-Cessa, JiangHua Feng, Nirwan Ansari, MengChu Zhou, and Tairan Zhang. "Beam with adaptive divergence angle in free-space optical communications for high-speed trains." arXiv preprint arXiv:1812.11233 (2018).
[29] Boone, B.G., Bruzzi, J.R., et al. (2004). Optical Communications Development for Spacecraft Applications. Johns Hopkins Apl Technical Digest, 25(4), 306−315.
[30] Mikołajczyk, Janusz, Zbigniew Bielecki, Maciej Bugajski, Józef Piotrowski, Jacek Wojtas, Waldemar Gawron, Dariusz Szabra, and Artur Prokopiuk. "Analysis of free-space optics development." Metrology and Measurement Systems 24, no. 4 (2017).
[31] M. Ali, “Performance analysis of fog effect on free space optical communication system,” IOSR Journal of Applied Physics (IOSR-JAP), vol. 7, pp. 16-24, 2015.
[32] Ghoname, Sherif, Heba A. Fayed, Ahmed Abd El Aziz, and Moustafa H. Aly. "Performance analysis of FSO communication system: Effects of fog, rain and humidity." In 2016 Sixth International Conference on Digital Information Processing and Communications (ICDIPC), pp. 151-155. IEEE, 2016.
[33] Bishop, C. M., & Nasrabadi, N. M. (2006). Pattern recognition and machine learning (Vol. 4, No. 4, p. 738). New York: springer.
[34] Mahesh, B. (2020). Machine learning algorithms-a review. International Journal of Science and Research (IJSR).[Internet], 9, 381-386.
[35] Ranstam, J., & Cook, J. A. (2018). LASSO regression. Journal of British Surgery, 105(10), 1348-1348.
[36] McDonald, G. C. (2009). Ridge regression. Wiley Interdisciplinary Reviews: Computational Statistics, 1(1), 93-100.
[37] T. Gunasegaran and Y. -N. Cheah, "Evolutionary cross validation," 2017 8th International Conference on Information Technology (ICIT), Amman, Jordan, 2017, pp. 89-95, doi: 10.1109/ICITECH.2017.8079960.
[38] S. Brindha, K. Prabha and S. Sukumaran, "A survey on classification techniques for text mining," 2016 3rd International Conference on Advanced Computing and Communication Systems (ICACCS), Coimbatore, India, 2016, pp. 1-5, doi: 10.1109/ICACCS.2016.7586371.
[39] M. Al Hamad and A. M. Zeki, "Accuracy vs. Cost in Decision Trees: A Survey," 2018 International Conference on Innovation and Intelligence for Informatics, Computing, and Technologies (3ICT), Sakhier, Bahrain, 2018, pp. 1-4, doi: 10.1109/3ICT.2018.8855780.
[40] Z. Zhang, Nady and M. Zhang, "Application of Decision Tree in Classification of Urban Firefighting," 2022 IEEE 10th Joint International Information Technology and Artificial Intelligence Conference (ITAIC), Chongqing, China, 2022, pp. 568-572, doi: 10.1109/ITAIC54216.2022.9836645.
[41] Suthaharan, S. (2016). Decision tree learning. In Machine Learning Models and Algorithms for Big Data Classification (pp. 237-269). Springer, Boston, MA.
[42] Ghazy, A. S., Selmy, H. A., & Shalaby, H. M. (2016). Fair resource allocation schemes for cooperative dynamic free-space optical networks. Journal of Optical Communications and Networking, 8(11), 822-834.
[43] Li, Yuan, Nikolaos Pappas, Vangelis Angelakis, Michał Pióro, and Di Yuan. "Optimization of free space optical wireless network for cellular backhauling." IEEE Journal on Selected Areas in Communications 33, no. 9 (2015): 1841-1854.
[44] World Weather API and Weather Forecast, Available at: https://www.worldweatheronline.com
[45] Google,” Google Earth”, Available at: https://earth.google.com/